Paper No. 15-1097

Quantitative Method for Assessing Deterioration Level of Wood Guardrail Posts

Chuck Plaxico
RoadSafe, LLC
Box 312
12 Main Street
Canton, Maine 04221
Phone: (614) 578-1942, e-mail: chuck@roadsafellc.com
Malcolm H. Ray
RoadSafe, LLC
Box 312
12 Main Street
Canton, Maine 04221
Phone: (207) 514-5474, e-mail: mac@roadsafellc.com

Word count
Text = 3,715
Figures & Tables: 14 @ 250 words each =3,500
Total number of words= 7,215

Submitted
August 1, 2015

Paper prepared for consideration for presentation and publication at the
94th Annual Meeting of the Transportation Research Board, January 2015

Paper No. 15-1097

Quantitative Method for Assessing Deterioration Level of Wood Guardrail Posts

Chuck A. Plaxico and Malcolm H. Ray

ABSTRACT

This paper presents the results of a study for developing an in-situ procedure for measuring the amount of deterioration of guardrail posts. The guardrail posts used in this study were extracted from damaged guardrail installations. The deterioration levels of the posts ranged from severe to essentially undamaged. A resistograph drilling device was used to measure the resistance of a 1/16-inch bit passing through the cross-section of the posts. A procedure was then developed to convert the resistograph data to a quantifiable deterioration score. Physical impact tests were then performed to correlate the degree of deterioration to the dynamic strength properties of the posts.

KEYWORDS: Guardrail Posts, Wood Deterioration, W-beam Guardrail, Pendulum Testing, Resistograph Testing.

INTRODUCTION

The guardrail post is a fundamental component of a guardrail system and its response during a crash event is important to the overall performance of the system. Wood posts are subject to decay and rot from several causes. The area at and just below the ground line is of great concern because the combination of moisture and air greatly promotes decay. Wood posts are also subject to inhabitation by ants and other small insects. The degradation of wood fibers takes place because insects create living space within the wood or by ingesting wood fibers for nutrients; in which case damage can occur within any portion of the wood post. There is no particular standard at this time for quantifying the degree of rot or deterioration in a guardrail post. The approach typically used is to simply replace any post with visible deterioration under the assumption that if rot is visible there is probably also a great deal of non-visible rot, especially just below the groundline.

The power industry has experienced similar problems with wooden utility poles. Like guardrail posts, utility poles remain in service for many years and can sometimes rot and deteriorate, often below ground. There are some destructive test techniques that involve drilling multiple large (e.g., ¾-inch diameter) holes in the pole and probing the interior but this would too greatly compromise strength if applied to guardrail posts. Several non-destructive techniques have been developed which have demonstrated reasonable accuracy in predicting breaking strength of utility poles based on the modulus of elasticity of the pole. These methods include static bending tests, stress wave propagation techniques, near infrared spectroscopy, and ultrasound to name a few.[*Hron11; Tallavo09; Green06; Hendrick03; Hascall07*] Another type of "non-destructive" test, which is the focus of this paper, involves the use of a resistograph, which measures the torque of a 1/16" diameter drill bit as it is inserted into the wood. The torque is measured as a function of length along the drill bit so any interior rot, voids or areas of low density are reflected in the torque measurement. The results are compared to a baseline reading on healthy wood to determine level of degradation. The resistograph can also drill at a 45 degree angle to obtain an indication of the subsurface condition of the post. Since the drill bit is only 1/16-inch diameter it is not considered a destructive test and there is little negative effect on the post strength due to the very small size hole.

The objective of this study was to develop a quantitative procedure for measuring the amount of deterioration of guardrail posts *in-situ*. The basic research approach entailed: (1) obtaining field-extracted wood guardrail posts from State DOT maintenance garages, (2) measuring the degree of deterioration of the posts with a Resistograph, (3) performing pendulum impact tests to measure the strength and capacity of the posts with various levels of deterioration, and (4) processing the pendulum tests and resistograph data to correlate levels of deterioration to strength degradation. The final step, which has been published elsewhere, is to quantify the effects of various levels of post deterioration on overall guardrail crash performance.[*Ray15*, *Plaxico15*]

TEST ARTICLES

The Ohio Department of Transportation (ODOT) provided 140 round wooden guardrail posts with various levels of deterioration for the physical test program. These posts were extracted from damaged guardrail installations in Ohio. The posts had round cross-sections with nominal diameter of 8 inches. The actual diameter varied from 6.45 inches to 9.15 inches with standard deviation of 0.62 inches. The post lengths varied from 5 to 6 ft, with the two most common lengths being 66 inches and 70 inches. In addition to the deteriorated posts, ODOT also donated three new (or unused) guardrail posts so that the Resistograph measurements from the in-service posts could be compared directly to the corresponding values for new posts.

RESISTOGRAPH MEASUREMENTS

The deterioration of each post was measured using an IML Resi-F400 S resistograph, shown in Figure 1. The resistograph was equipped with a 1/16 inch in diameter drilling needle 19 $^{5}/_{16}$ inches long. The resistograph measurements were recorded at increments of approximately 0.004 inches of drilling depth. The measurements were taken just below, or at, the groundline where the highest levels of deterioration were visually evident. With the posts extracted from ground, this critical area of the post was readily accessible, so the measurements were made at 90 degrees to the post.

Figure 1. IML Resi-F400 S Resistograph

Resistograph Data Processing and Interpretation

The data from the resistograph was then processed to develop a procedure to yield a single quantitative value representing the strength or capacity of the posts. The pendulum test program, which will be discussed later, involved the post mounted in a rigid foundation, in which the guardrail post was essentially a cantilevered beam with a concentrated load applied at the end of, and normal to, the post. The stresses in the post arise from the resulting bending moment, where

the stress profile through the cross-section of a beam in pure bending can be calculated from the following equation:

$$\sigma = \frac{Mc}{I}$$

Where *M* is the bending moment, *I* is the moment of inertia of the beam, and *c* is the distance from the neutral axis of the beam. Since *M* and *I* are constants, the strain varies linearly through the cross-section, increasing from zero at the neutral axis to a maximum value at the outermost fiber of the beam. If the material is elastic and homogeneous then the stress also varies linearly through the cross-section. For a non-homogeneous material such as wood, on the other hand, the stress values vary through the cross-section as a function of the local wood modulus, as illustrated in the schematic in Figure 2.

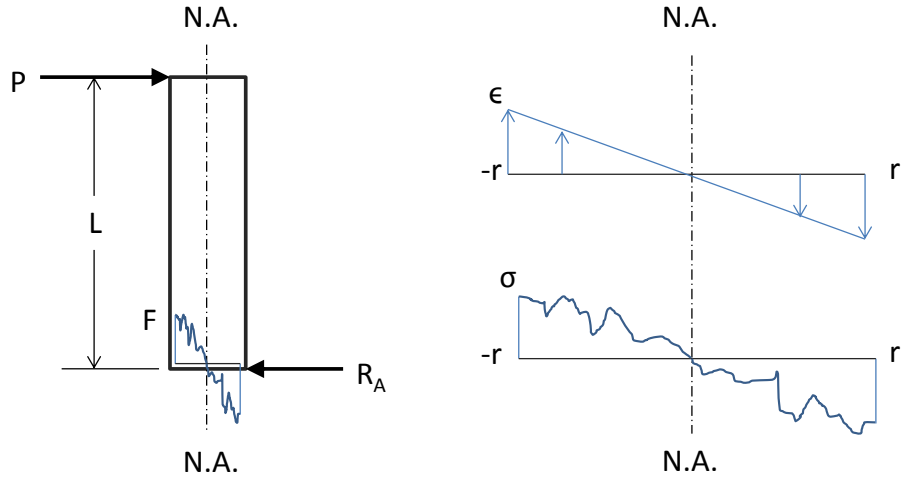

Figure 2. Schematic of typical (a) Free-body and (b) strain and stress diagrams for non-homogeneous beam under bending load (positive in compression).

From the free body diagram in Figure 2, equilibrium is achieved when the sum of the moments due to the internal forces at Point A are equal to the moment created by the applied force P times its distance L, as described by:

$$\int_{-r}^{r} F dy = PL$$

If the internal force at Point A in Figure 2 is approximated in terms of discrete forces, F_i, acting at fixed increments, y_i, through the cross-section of the post, as illustrated in Figure 3, then the equilibrium condition can be re-written as:

$$\sum_{i=1}^{N} F_i y_i = PL$$

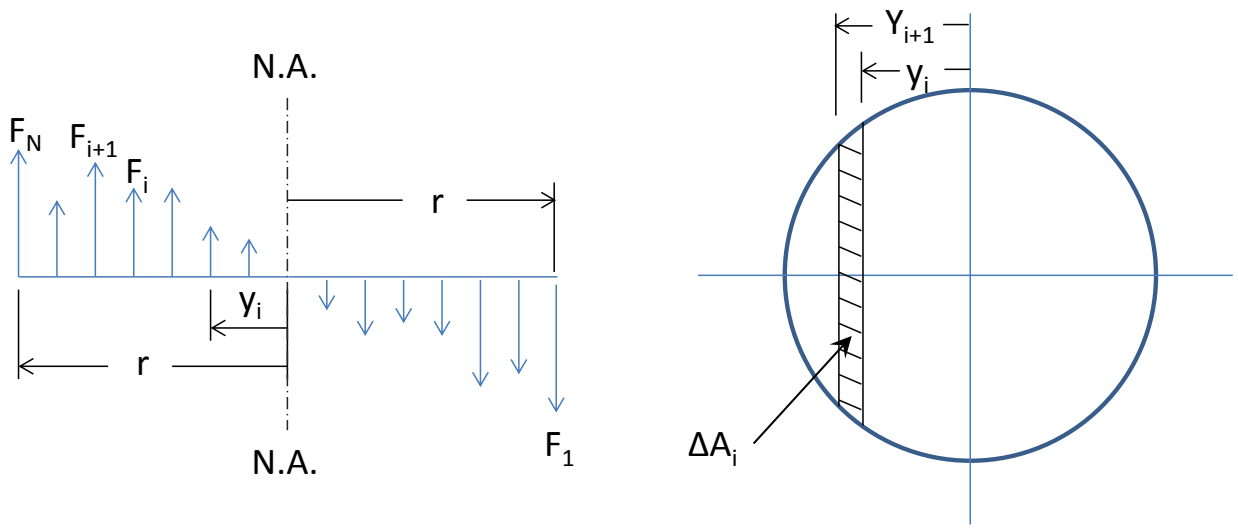

Figure 3. Schematic illustrating internal force distribution through cross-section of a circular shaped post.

Figure 4 shows the resistograph results for one of the new posts (i.e., Post A), illustrating a typical torque vs. depth plot through the cross section of a guardrail post. It is assumed that the torque resistance amplitude at each point is directly proportional to the modulus (or strength) of the post fibers at that location. Thus, for a given applied load, each data point from the resistograph can be converted to a "pseudo" force value using the following equation:

$$F_i^* = E_i^* A_i \frac{y_i}{r}$$

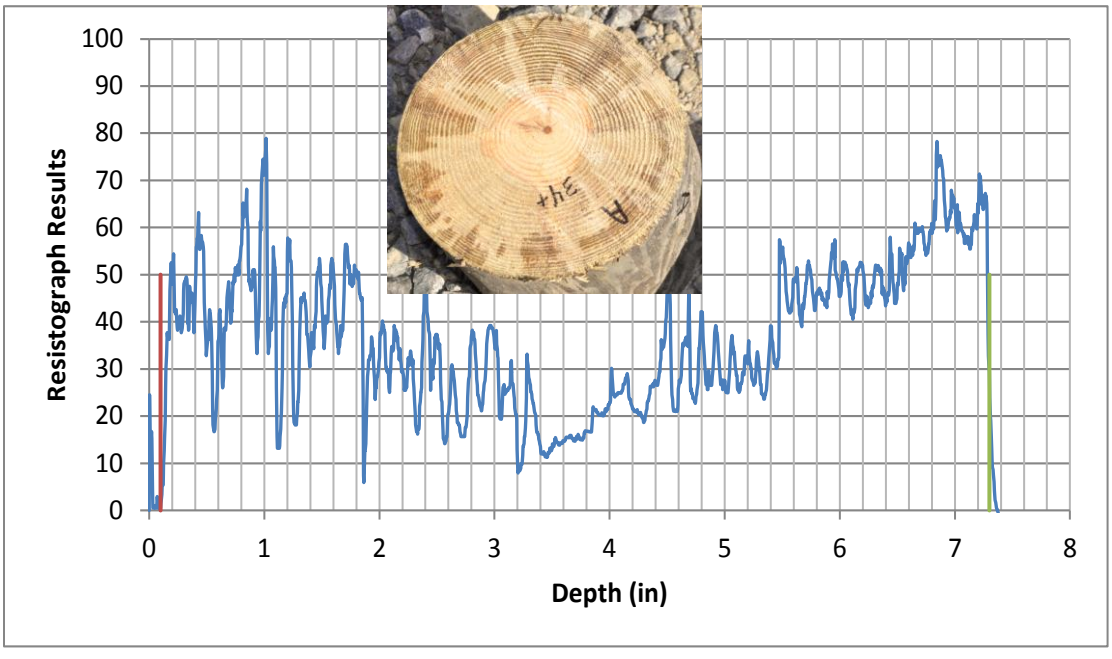

Figure 4. Resistograph results for Post A.

Where, F_i^* are the pseudo forces, E_i^* are pseudo modulus values, ΔA_i is the incremental area over which each force acts, y_i is the distance of the force from the neutral axis of the post, and r is the radius of the post. For a circular section ΔA_i can be approximated as:

$$\Delta A_i = (y_{i+1} - y_i)\left(\sqrt{r^2 - y_i^2} + \sqrt{r^2 - y_{i+1}^2}\right)$$

The total resisting "moment" of the post is then proportional to the pseudo moment defined by:

$$M^* = \sum_i E_i^* A_i \frac{y_i^2}{r}$$

The maximum stress in the beam, often referred to as the modulus of rupture (MOR), is computed for a circular post as follows:

$$MOR = \sigma_{max} = \frac{M}{S} = \frac{M}{\left(\frac{\pi r^3}{4}\right)}$$

Where S is the section modulus. Substituting the pseudo modulus, M^*, for M in the above equation results in a pseudo modulus of rupture, MOR^*, defined by:

$$MOR^* = \frac{4M^*}{\pi r^3} = \frac{4}{\pi r^4}\sum_i E_i^* A_i y_i^2 \quad \textbf{(1)}$$

The energy absorbed by the post at onset of rupture as well as the amount of energy required to fully rupture the post are also meaningful values for quantifying the performance of a guardrail post. The constitutive behavior of wood is assumed linear for calculation of the strain energy (for the sake of simplification), which yields:

$$U = \int \sigma \varepsilon dV \approx \sum_i \sigma_i \epsilon_{i=} \sum_i E_i \epsilon_i^2 = \sum_i E_i \frac{y_i^2}{r^2}$$

Thus, a pseudo strain energy can be computed for the post by substituting E^* for E in the above equation such that:

$$U^* = \frac{1}{r^2}\sum_i E_i^* y_i^2 \quad \textbf{(2)}$$

Resistograph Score

The following discusses the procedure used to convert the resistograph results to a single quantitative value that represents the strength capacity of the posts. The strength capacity "score" was defined in terms of two strength quantities: (1) a score representing the pseudo modulus of rupture, S_{MOR*} and (2) a score representing energy capacity, S_{U*}.

Procedure for Computing S_{MOR*}

From Eq(1):

1. Compute $A_i y_i^2$

2. Divide each $A_i y_i^2$ value by the cumulative sum of $\sum_i A_i y_i^2$ values, to obtain an individual weight for each E_i^* value, such that the sum of all the individual weights is unity, i.e.,

$$\sum_i \frac{A_i y_i^2}{\sum_j A_j y_j^2} = 1$$

3. Multiply each torque amplitude, E_i^*, by its corresponding weight and sum all the weighted torque amplitudes to obtain a single cumulative weighted score, i.e.,

$$\sum_i \frac{E_i^* A_i y_i^2}{\sum_j A_j y_j^2}$$

4. Corresponding to the term on the outside of the summation in Eq(1), the weighted score is then scaled by a shape factor equal to the square of the measured post radius normalized with respect to the nominal radius of 4 inches, i.e.,

$$\frac{\frac{4}{\pi(4)^4}}{\frac{4}{\pi r^4}} = \left(\frac{r}{4}\right)^4$$

5. The effective strength capacity score, S_{MOR^*}, corresponding to the modulus of rupture for the post is then:

$$S_{MOR^*} = \left(\frac{r}{4}\right)^4 \sum_i \frac{E_i^* A_i y_i^2}{\sum_j A_j y_j^2} \quad \textbf{(3)}$$

Procedure for Computing S_{U^*}

From Eq(2):

1. Compute y_i^2
2. Divide each y_i^2 value by the cumulative sum of $\sum_i y_i^2$ values, to obtain an individual weight for each E_i^* value, such that the sum of all the individual weights is unity, i.e.,

$$\sum_i \frac{y_i^2}{\sum_j y_j^2} = 1$$

3. Multiply each torque amplitude, E_i^*, by its corresponding weight and sum all the weighted torque amplitudes to obtain a single cumulative weighted score, i.e.,

$$\sum_i \frac{E_i^* y_i^2}{\sum_j y_j^2}$$

4. Corresponding to the term on the outside of the summation in Eq(2), the weighted score is then scaled by a shape factor equal to the square of the measured post radius normalized with respect to the nominal radius of 4 inches, i.e.,

$$SF = \frac{\frac{1}{(4)^2}}{\frac{1}{r^2}} = \left(\frac{r}{4}\right)^2$$

5. The effective strength capacity score, S_{U^*}, corresponding to the rupture energy of the post is then:

$$S_{U^*} = \left(\frac{r}{4}\right)^2 \sum_i \frac{E_i^* y_i^2}{\sum_j y_j^2} \quad \textbf{(4)}$$

Equations (3) and (4) provide quantitative metrics that represent a relative capacity of a round guardrail post in terms of modulus of rupture (i.e., maximum stress) and strain energy capacity, respectively. Both of these metrics increase as the torque amplitude value, E_i^*, increases and as the radius of the post increases, thus the higher metric values indicate higher capacity. The resulting S_{MOR^*} and S_{U^*} values will later be correlated to the pendulum test results to develop a relationship(s) for estimating the dynamic strength properties of wood guardrail posts.

PENDULUM TESTING OF POST-IN-RIGID-FOUNDATION

Pendulum tests were conducted to assess the dynamic failure properties of the deteriorated posts. The tests were performed by the staff of the Federal Outdoor Impact Laboratory (FOIL) at the Federal Highway Administration's Turner Fairbank Highway Research Center in McLean, Virginia. The tests involved a 2,372-lb rigid pendulum impacting the posts at a nominal impact speed of 10 mph at a height of 21.5 inches above ground. A total of 39 tests were conducted; the complete test matrix is shown below in Table 1.

In order to reduce the effects of moisture content, each wood post specimen was saturated prior to testing. Each specimen was cut to 66 inches long, weighed, and then soaked for several hours in an open water tank. Only the portion of the posts that were to be embedded into the steel sleeve (i.e., below groundline) was submerged in the tank to achieve realistic saturation of the posts (i.e., saturation below the groundline and air-dried above the groundline). The pre-soaked post specimens were again weighed just prior to testing. The circumferences of the posts were measured at the top, at the groundline and at the bottom of the posts to estimate the average diameter of the post. The average diameter, post length and weight of the post were then used to calculate the wet density for each post. The number of rings for each post was counted and used to determine the average ring density for each post. The moisture content was measured immediately after each pendulum test at several points through the cross-section of the post along the break-line using an MT-10 moisture meter developed by AMPROBE. The moisture meter was not able to obtain accurate readings when the moisture content exceeded 50 percent. In those cases the moisture content was reported as "greater than 50 percent".

Table 1. Test matrix for pendulum test series 13009.

Test No.	Test Date	Post No.	Length (in)	Initial Weight (lbs)	Soak Time (hours)	Soak Weight (lbs)	Circumference bottom (in)	Circumference mid (in)	Circumference top (in)	Volume (in3)	Wet Density (lb/ft3)	Groundline Diameter (in)	Number of Rings	Ring Density (rings/in)
13009Y	10/1/2013	43	66.0	65.0	17.0	85	24.3	23.8	24.3	3046.3	48.2	7.6	22	5.8
13009Z	10/1/2013	56	66.0	71.0	18.5	92	25.5	25.8	24.8	3370.7	47.2	8.1	30	7.4
13009A1	10/1/2013	50	66.0	69.0	19.0	74	24.5	23.0	25.5	3109.8	41.1	7.4	47	12.7
13009B1	10/1/2013	31	66.0	59.0	19.5	70	23.5	24.3	24.3	3025.2	40.0	7.6	17	4.5
13009C1	10/1/2013	47	66.0	69.0	20.0	93	27.0	25.5	24.8	3482.5	46.1	8.0	27	6.8
13009D1	10/1/2013	55	66.0	51.0	20.5	63	22.3	22.5	23.5	2718.3	40.0	7.3	26	7.1
13009E1	10/1/2013	32	60.0	103.0	21.0	119	26.8	26.8	27.8	3502.2	58.7	8.8	26	5.9
13009F1	10/1/2013	88	60.0	41.0	21.5	56	23.0	23.8	24.3	2674.3	36.2	7.6	20	5.3
13009G1	10/2/2013	71	60.0	61.0	18.0	70	26.0	23.5	23.3	2807.8	43.1	7.6	30	7.9
13009H1	10/2/2013	30	60.0	67.0	18.5	73	26.0	25.3	24.5	3044.1	41.4	8.0	28	7.0
13009I1	10/2/2013	76	60.0	70.0	19.0	75	28.3	26.3	25.5	3395.3	38.2	8.4	30	7.2
13009J1	10/2/2013	49	66.0	70.0	19.5	76	26.3	24.3	23.3	3174.1	41.4	7.5	30	8.0
13009K1	10/2/2013	29	66.0	72.0	20.0	80	23.0	22.0	23.3	2718.3	50.9	7.0	25	7.1
13009L1	10/2/2013	92	66.0	74.0	20.5	78	25.5	25.3	23.8	3239.0	41.6	8.0	32	8.0
13009M1	10/2/2013	68	66.0	65.0	21.0	69	24.0	23.3	22.8	2859.5	41.7	7.4	35	9.5
13009N1	10/3/2013	17	66.0	71.0	18.0	76	25.0	25.5	25.5	3370.7	39.0	8.0	30	7.5
13009O1	10/3/2013	94	66.0	37.0	18.5	47	21.3	20.8	20.8	2297.8	35.3	6.6	20	6.1
13009P1	10/3/2013	44	66.0	61.0	19.0	80	24.0	23.3	23.0	2879.9	48.0	7.6	30	7.9
13009Q1	10/3/2013	53	66.0	52.0	19.5	68	25.0	24.3	25.8	3282.6	35.8	7.6	24	6.3
13009R1	10/3/2013	84	66.0	72.0	20.0	84	24.5	22.3	22.5	2798.5	51.9	6.6	30	9.1
13009S1	10/3/2013	21	66.0	97.0	20.5	109	29.0	25.8	23.8	3596.1	52.4	8.0	50	12.6
13009T1	10/3/2013	63	66.0	57.0	21.0	62	24.0	23.5	23.5	2941.8	36.4	7.5	30	8.0
13009U1	10/3/2013	65	60.0	58.0	21.5	68	26.3	24.3	23.5	2905.1	40.4	7.6	32	8.4
13009V1	10/8/2013	90	66.0	37.0	18.0	49	21.8	22.3	22.5	2580.7	32.8	7.0	16	4.6
13009W1	10/8/2013	118	66.0	63.0	18.5	79	25.3	25.5	24.8	3326.5	41.0	7.7	28	7.3
13009X1	10/8/2013	81	66.0	69.0	19.0	87	24.0	22.5	22.3	2758.3	54.5	6.7	22	6.6
13009Y1	10/8/2013	123	66.0	74.0	19.5	92	26.0	26.3	25.0	3482.5	45.7	8.3	19	4.6
13009Z1	10/8/2013	61	66.0	73.0	20.0	90	27.0	26.0	27.0	3734.8	41.6	8.2	25	6.1
13009A2	10/8/2013	67	66.0	68.0	20.5	83	25.5	25.5	26.0	3460.0	41.5	8.2	21	5.1
13009B2	10/8/2013	126	66.0	77.0	21.0	93	25.8	26.3	26.0	3550.4	45.3	8.3	29	7.0
13009C2	10/8/2013	91	66.0	76.0	22.5	93	27.5	27.0	25.5	3734.8	43.0	8.6	37	8.6
13009D2	10/9/2013	105	66.0	52.0	17.0	63	24.0	23.0	22.8	2839.1	38.3	7.0	17	4.9
13009 E2	10/9/2013	117	66.0	73.0	17.5	81	27.0	27.0	26.5	3781.7	37.0	8.6	25	5.8
13009F2	10/9/2013	129	66.0	58.0	18.0	79	23.0	23.0	23.3	2798.5	48.8	7.3	28	7.7
13009G2	10/9/2013	24	66.0	81.0	18.5	84	25.3	25.8	27.3	3573.2	40.6	8.4	30	7.1
13009H2	10/9/2013	35	66.0	83.0	19.0	86	26.8	25.5	25.0	3482.5	42.7	8.1	22	5.4
13009I2	10/9/2013	78	66.0	68.0	19.5	78	23.5	24.0	26.0	3152.6	42.8	7.6	24	6.3
13009J2	10/9/2013	111	66.0	68.0	20.0	71	24.0	24.5	24.8	3131.2	39.2	7.6	28	7.4
13009K2	10/9/2013	114	60.0	63.0	20.5	69	24.3	25.0	25.0	2924.8	40.8	8.0	35	8.8

Test Specimen Mounting Condition

The tests were performed with the posts installed in a rigid steel sleeve, as shown in Figure 5. The sleeve was a 12 x 12 x ¼ inch steel tube fabricated from A500 Class B 58,000 psi structural steel. The top of the tube was reinforced with a 5-inch tall 13 x 13 x ½ inch steel tube welded to the main tube sleeve. The foundation sleeve was braced against the steel reinforced concrete wall on the inside of the ground-pit using a 7.4 ft long S20x86 structural steel section. The posts were mounted inside the sleeve at a nominal depth of 38 inches, except for the few cases in which the length of the post was too short (e.g., several of the posts were only 60 inches long, which resulted in an embedment of 32 inches). In all cases, the top mounting height of the posts was nominally 28 inches. The posts were held in place inside the sleeve using structural grade pine boards (e.g., 2x8) that were press-fit against the back-side of the sleeve using a 1.0-inch diameter grade 8 set-screw.

Figure 5. Rigid steel sleeve used for post mounting.

Pendulum Device

The striker for the tests was a 2,372-lb concrete pendulum with a semi-rigid nose. The semi-rigid nose, which was developed by researchers from Virginia Tech during the first phase of this study, was fabricated from a wooden block and covered with sheet metal (see Figure 5).[Gabler10] The radius of chamfer at the center of the impactor face was 6 inches, which was based on measurements of a 2006 Chevrolet 1500 pickup truck. [Gabler10]

The pendulum was instrumented with three accelerometers mounted onto the backside of the pendulum mass. Two of the accelerometers recorded data in the x-direction (forward direction) and the third accelerometer recorded data in the z-direction (vertical direction). The tests were also recorded using four high-speed cameras with an operating speed of 500 frames per second and a digital video camera (~30 fps).

Results

Table 2 provides the peak force, the strain energy at initiation of rupture, peak moment, and the energy at complete rupture for each post in Test Series 13009. For the 39 tests, the peak force ranged from 3.25 kips to 18.4 kips, with mean of 9.32 kips and standard deviation of 3.75 kips. The strain energy of the post at the point of initial rupture ranged from 4 kip-in to 43.3 kip-in, with mean of 21.4 and standard deviation 11.5. The total energy absorbed by the post at the point of complete rupture ranged from 5.44 kip-in to 80.6 kip-in, with mean of 27.7 and standard deviation of 16.0. These statistics are summarized in Table 3.

Figure 6 shows a plot of the peak impact force vs. S_{MOR}; Figure 7 shows a plot of the strain at initiation of rupture vs. S_{U*}; and Figure 8 shows a plot of the rupture energy vs. S_{U*}. The linear regression of the data for the peak force and peak moment curves yielded R^2 values of 0.69 and 0.68, respectively, which indicated that both curves fit the data reasonably well. The linear regression fit of the energy at rupture initiation yielded an R^2 value of 0.67, which indicated that this curve was also a reasonable fit. The linear regression for the rupture energy data yielded R^2 value of 0.46 which indicated a significant scatter in the data. From visual inspection, however, it seems apparent that the rupture energy does indeed increase somewhat linearly with respect to S_U, with the exception of three data points, which correspond to tests

13009Q1, 13009T1 and 13009Y1. In test 13009Q1, the post had an S_U value of 27.6 but resulted in a rupture energy of 7.8 kip-inches which was among the lowest rupture energies of all posts tested. Likewise, Tests 13009T1 and 13009Y1 involved posts with S_U values of 33.1 and 29.8, respectively, but resulted in greater rupture energy than any other posts tested. In fact, the post in Test 13009Y1 stopped the pendulum without fully rupturing the post. These cases are highlighted in red font in Table 2. Excluding those three data points from the plot for rupture energy vs. S_U, resulted in a reasonable fit to the remaining data with an R^2 value of 0.74, as shown in Figure 8.

Table 2. Test Results for Test Series 13009.

Test No.	Test Date	Post No.	Ring Density	Ground-Line (in)	Moisture Content (%)	Weight (lb)	Resistograph Score		At Peak Force				Rupture Energy (kip-in)
							SMOR	SU	Force (kip)	Deflection (in)	Energy (kip-in)	Moment kip-in	
13009Y	10/1/2013	43	5.8	7.6	-999.0	85	21.9	26.9	9.9	2.5	12.7	230.8	18.1
13009Z	10/1/2013	56	7.4	8.1	45.1	92	27.7	27.7	7.6	3.8	21.3	194.3	24.3
13009A1	10/1/2013	50	12.7	7.4	-999.0	74	15.9	17.5	6.9	2.8	8.2	158.6	12.8
13009B1	10/1/2013	31	4.5	7.6	-999.0	70	3.5	6.0	4.2	2.4	6.4	97.6	7.6
13009C1	10/1/2013	47	6.8	8.0	0.0	93	23.4	27.9	5.2	2.7	16.4	127.3	18.4
13009D1	10/1/2013	55	7.1	7.3	37.7	63	19.5	25.4	8.8	3.0	15.0	228.3	21.6
13009E1	10/1/2013	32	5.9	8.8	-999.0	119	48.3	44.3	15.4	4.7	38.4	402.0	43.8
13009F1	10/1/2013	88	5.3	7.6	-999.0	56	3.0	4.5	4.9	3.6	10.6	108.4	10.8
13009G1	10/2/2013	71	7.9	7.6	42.2	70	28.2	32.1	9.5	2.5	26.9	230.6	30.9
13009H1	10/2/2013	30	7.0	8.0	43.6	73	34.8	37.2	12.2	3.5	41.2	288.2	45.7
13009I1	10/2/2013	76	7.2	8.4	47.6	75	47.0	47.7	18.4	5.1	42.4	412.7	42.5
13009J1	10/2/2013	49	8.0	7.5	36.6	76	14.0	15.1	9.8	2.4	18.4	247.9	24.8
13009K1	10/2/2013	29	7.1	7.0	50.0	80	18.3	27.4	7.8	3.9	20.7	193.3	24.3
13009L1	10/2/2013	92	8.0	8.0	44.5	78	51.9	50.6	13.7	4.0	36.6	339.1	42.9
13009M1	10/2/2013	68	9.5	7.4	47.2	69	32.8	41.1	14.8	4.4	32.0	354.8	34.9
13009N1	10/3/2013	17	7.5	8.0	48.0	76	17.1	17.1	7.3	2.2	12.9	162.7	16.2
13009O1	10/3/2013	94	6.1	6.6	50.0	47	7.2	11.9	3.8	2.1	5.3	86.7	6.3
13009P1	10/3/2013	44	7.9	7.6	50.0	80	13.8	18.6	9.3	3.5	22.3	257.5	22.9
13009Q1	10/3/2013	53	6.3	7.6	47.6	68	24.7	27.6	4.3	1.1	4.0	97.2	7.8
13009R1	10/3/2013	84	9.1	6.6	49.7	84	18.4	22.1	8.0	2.7	21.7	175.3	23.0
13009S1	10/3/2013	21	12.6	8.0	50.0	109	40.3	35.5	8.5	2.3	12.5	217.8	18.5
13009T1	10/3/2013	63	8.0	7.5	37.3	62	27.4	33.1	9.7	7.6	28.0	213.2	61.5
13009U1	10/3/2013	65	8.4	7.6	50	68	17.2	16.2	8.2	3.6	14.5	186.0	17.8
13009V1	10/8/2013	90	4.6	7.0	50	49	2.5	4.9	3.2	2.4	6.7	70.6	6.8
13009W1	10/8/2013	118	7.3	7.7	50	79	12.6	14.3	5.3	2.1	6.7	121.0	9.7
13009X1	10/8/2013	81	6.6	6.7	50	87	12.2	17.0	6.1	4.0	18.0	141.3	30.7
13009Y1	10/8/2013	123	4.6	8.3	50	92	30.8	27.6	9.2	3.2	19.4	217.8	80.6
13009Z1	10/8/2013	61	6.1	8.2	45.5	90	33.0	31.0	11.6	4.4	35.2	294.2	43.5
13009A2	10/8/2013	67	5.1	8.2	50	83	29.1	32.3	10.6	3.5	22.2	239.5	26.0
13009B2	10/8/2013	126	7.0	8.3	50	93	42.7	39.6	13.1	5.0	43.3	304.2	47.2
13009C2	10/8/2013	91	8.6	8.6	46.16	93	52.7	44.1	17.5	3.8	28.6	364.1	36.8
13009D2	10/9/2013	105	4.9	7	50	63	4.4	6.6	5.0	2.2	5.4	121.1	5.4
13009 E2	10/9/2013	117	5.8	8.6	46.2	81	15.0	15.4	9.6	3.5	18.2	227.5	18.3
13009F2	10/9/2013	129	7.7	7.25	50	79	11.8	16.9	6.5	3.4	13.4	165.0	19.9
13009G2	10/9/2013	24	7.1	8.4	50	84	28.1	25.8	12.6	3.6	27.4	290.4	29.6
13009H2	10/9/2013	35	5.4	8.1	50	86	31.1	30.1	7.0	2.2	22.2	160.3	25.8
13009I2	10/9/2013	78	6.3	7.6	36.28	78	41.1	40.7	13.8	5.0	39.5	330.4	44.5
13009J2	10/9/2013	111	7.4	7.6	50	71	25.3	32.5	12.8	4.0	28.8	309.3	40.4
13009K2	10/9/2013	114	8.8	8	47.84	69	31.8	33.4	11.6	4.6	31.9	268.8	33.3

Table 3. Statistics for Post Strength Capacity from Pendulum Test Series 13009.

Capacity Measure	Post Strength Statistics			
	Mean	Std. Dev.	Min	Max
Peak Force	9.32	3.75	3.25	18.44
Energy at Initial fracture	21.42	11.47	4.00	43.30
Energy at Complete Rupture	27.68	16.04	5.44	80.60

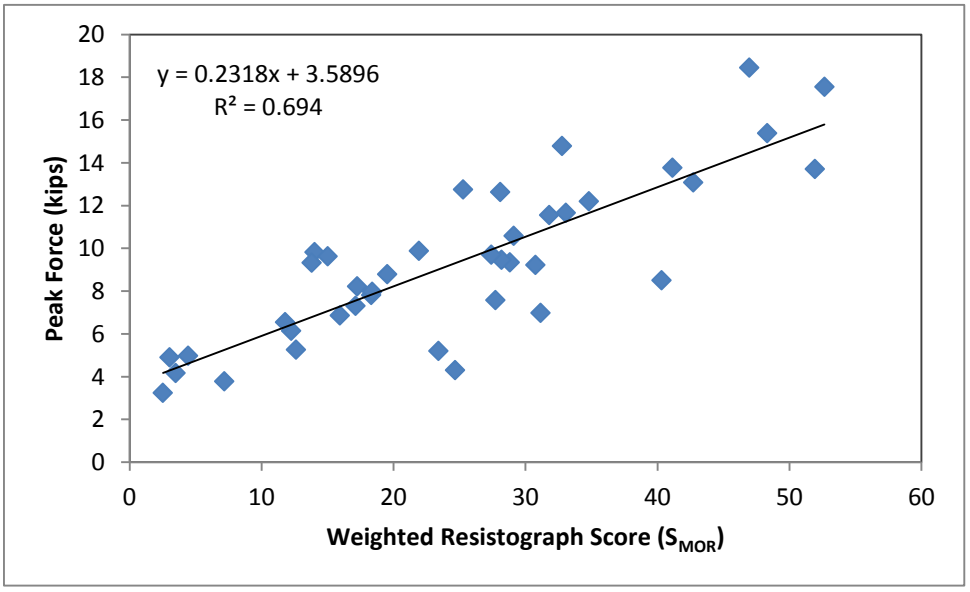

Figure 6. Peak Force vs. S_{MOR}.

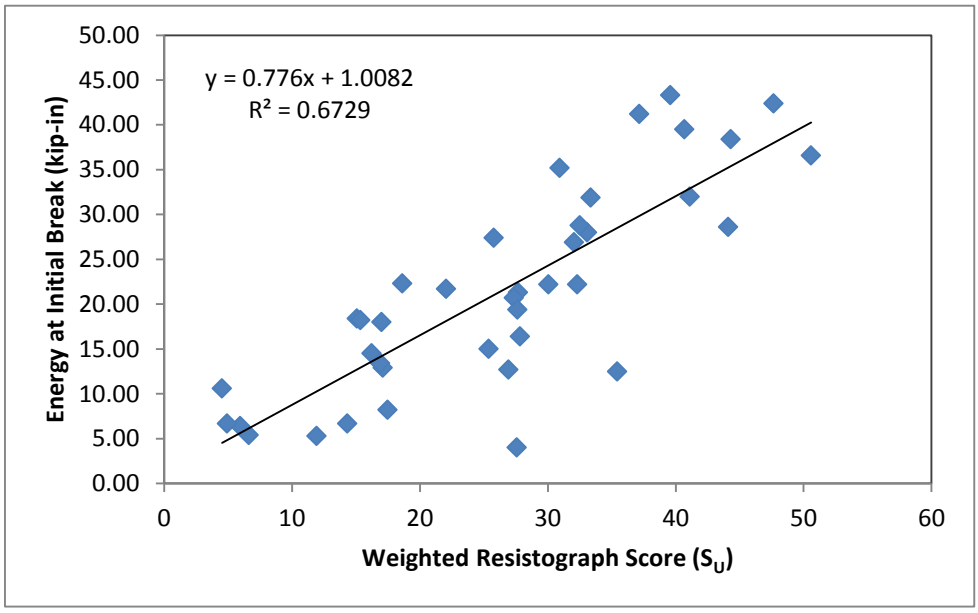

Figure 7. Energy at rupture initiation vs. S_U.

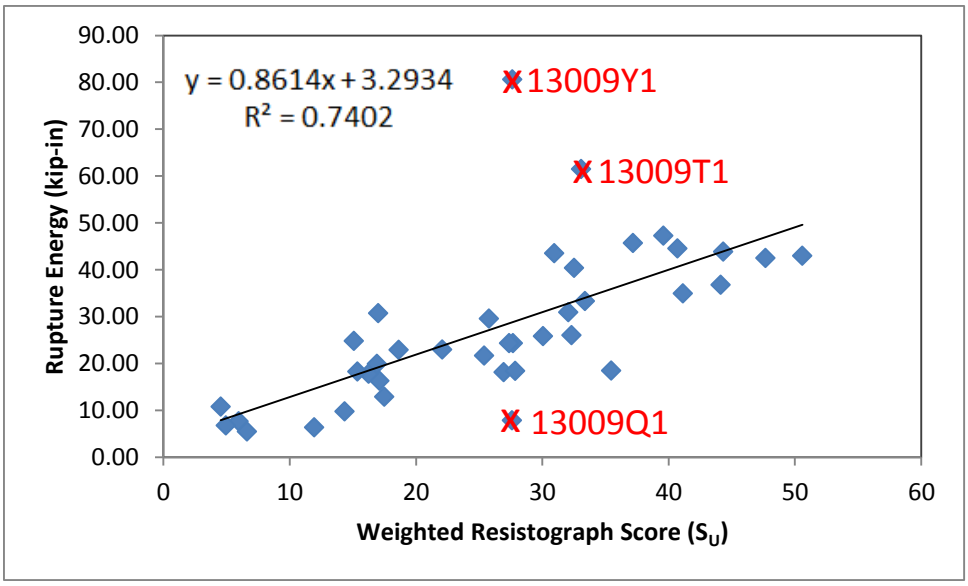

Figure 8. Rupture Energy vs. S_U (excluding Tests 13009Q1, Test 13009T1 and Test 13009Y1).

QUANTIFYING WOOD POST DETERIORATION DAMAGE LEVELS

Four levels of deterioration for wood guardrail posts were established based on the results of the pendulum impact and are defined in Table 4 in terms of force capacity, energy capacity and the weighted resistograph scores, S_u and S_{MOR}. Figures 9 shows the results from three tests performed in the 13009 test series that are representative of the three deterioration levels DL1, DL2 and DL3. Figure 10 shows a graphical representation of the damage levels with respect to resi-score, S_U, and strain energy capacity; Figure 11 shows a graphical representation of damage levels with respect to resi-score, S_{MOR}, and load capacity. The two resi-scores, S_U and S_{MOR}, are computed slightly differently, but the resulting scores corresponding to damage levels are very similar; thus, either may be used. The last column of Table 4 presents the damage levels of the post in terms of relative capacity. Therefore, if post strength is measured or otherwise determined in the field via alternative means (e.g., stress wave techniques, force-deflection techniques, etc.) then the relative capacity may be used to identify damage level.

Table 4. Damage levels for guardrail post deterioration.

	8-inch Round Posts (nominal)			General
	Capacity		Resi Score	
Damage Level	Peak Force (kips)	Strain Energy (kip-in)	S_U or S_{MOR}	Relative Capacity
0 (new)	> 14	> 35	> 45	100%
1	12 - 15	26 - 40	35-45	75%
2	7 - 13	20 - 30	25 - 35	55%
3	< 9	< 20	< 25	< 45%

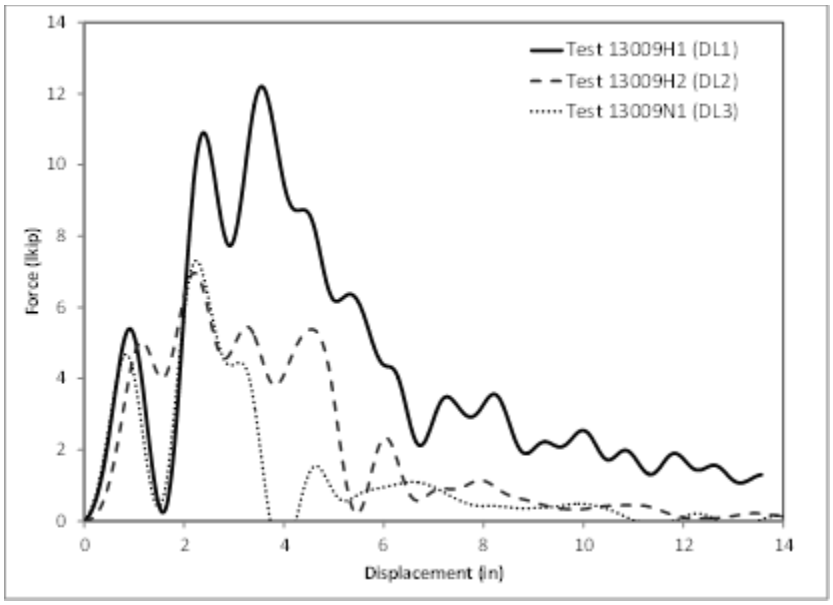

Figure 9. Pendulum test results corresponding to deterioration damage level.

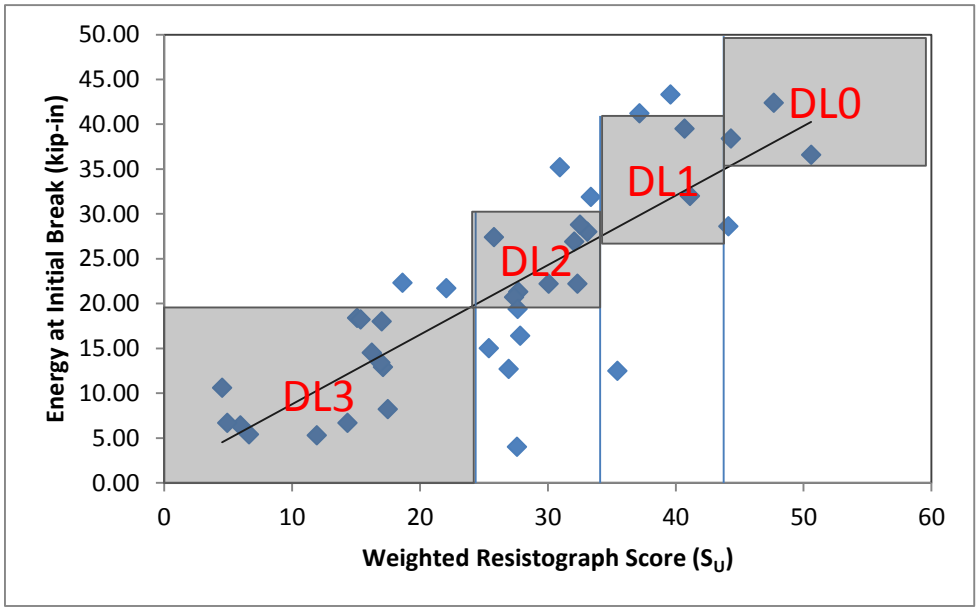

Figure 10. Graphical representation of damage levels with respect to resi-score, S_U, and strain energy capacity.

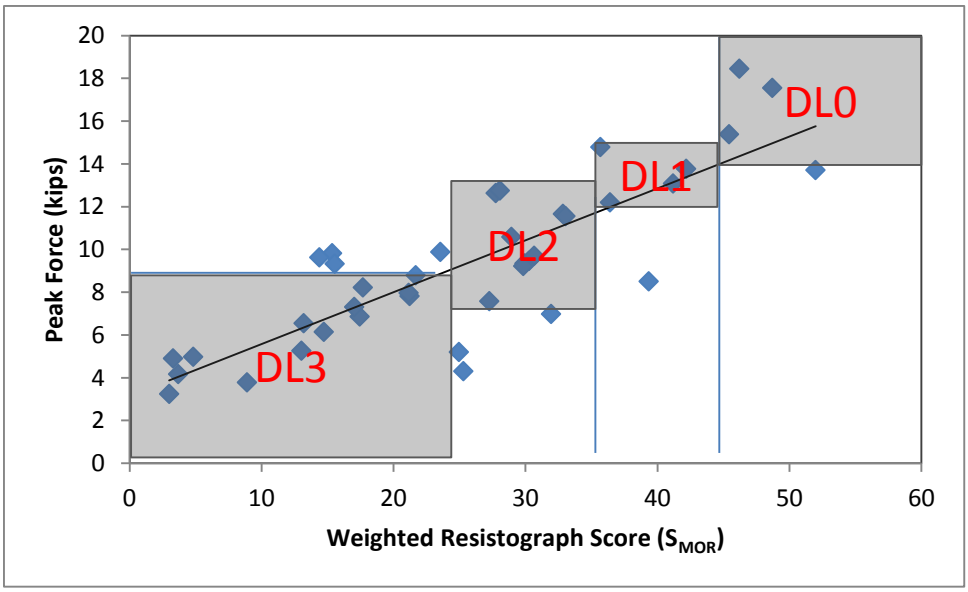

Figure 11. Graphical representation of damage levels with respect to resi-score, S_{MOR}, and load capacity.

SUMMARY AND CONCLUSIONS

The purpose of this study was to correlate guardrail post deterioration to the resulting strength degradation of the post. This was achieved by obtaining field-extracted posts from damaged guardrail installations in Ohio with deterioration levels ranging from severe to essentially undamaged; developing a procedure for quantifying the degree of deterioration; and correlating the degree of deterioration to the dynamic properties of the posts.

A resistograph device was used to quantify the degree of deterioration of each post by drilling a 1/16th inch diameter drill bit through the full diameter of each post at the groundline and recording the torque resistance on the drilling needle as a function of drilling depth. This information was then processed to determine a deterioration score that represented the effective degradation of post strength. The deterioration score was developed assuming that the resistograph data (i.e., torque amplitude on the drill bit) was linearly proportional to the local fiber strength (e.g., modulus) of the wood at each data point measured through the cross-section of the post. Accordingly, the resistograph data points were then weighted based on the effects of the measured strength and location within the cross-section with regard to the bending resistance and strain energy capacity of the post.

Pendulum tests were conducted to measure the dynamic impact response of the posts. The tests involved a 2,372-lb rigid pendulum impacting the posts at an impact speed of 10 mph and at a height of 21.5 inches above ground. The test data was found to correlate reasonably well with the resistograph scores. Based on a least-squares regression analysis of the data it was determined that the peak force, peak moment and rupture energy all increase as a linear function of the weighted resistograph score. There was, of course, some scatter in the data which was expected due to the many variables that affect wood strength. The effects of moisture, however,

were hopefully minimized in the tests since all the posts were soaked to saturation levels prior to testing.

A necessary next step is to quantify the effects of various levels of post deterioration on the crash performance of the guardrail system. The information developed herein would be directly applicable to such a study. The procedure for determining deterioration could be used to identify posts with specific deterioration levels for use in a full-scale test program. The results from the pendulum tests could be used to calibrate finite element models of wood posts with various levels of post deterioration, which could then be included in a validated model of the guardrail system. The latter has been implemented and published elsewhere.[*Ray15; Plaxico15*]

ACKNOWLEDMENTS

This paper was based on work performed as part of National Cooperative Highway Research Program (NCHRP) Project 22-28, "Criteria for Restoration of Longitudinal Barriers, Phase II." The authors would like to thank the NCHRP for its support and the NCHRP project staff and the project panel for their comments, suggestions and direction. The authors are also indebted to the Federal Highway Administration who fully sponsored the physical testing for this study which was performed at the Federal Outdoor Impact Laboratory (FOIL) at the Federal Highway Administration's Turner Fairbank Highway Research Center (TFHRC) in McLean, Virginia. The authors would also like to thank the Ohio Department of Transportation for supplying the aged/deteriorated guardrail posts for the study.

REFERENCES

Gabler10 Gabler, H.C., Gabauer, D.J., Hampton, "Criteria for Restoration of Longitudinal Barriers," NCHRP Report 656, Transportation Research Board, Washington, D.C. (2010).

Green06 Green, D.W., T.M. Gorman, J.W. Evans, and J.F. Murphy, "Mechanical Grading of Round Timber Beams," Journal of Materials in Civil Engineering, American Society of Civil Engineers, Vol 18, pg 1-9 (2006).

Hascall07 Hascall, J.A., R.K. Faller, J.D. Reid, D.L. Sicking, and D.E. Kretschmann, " Investigating the Use of Small-Diameter Softwood as Guardrail Posts (Dynamic Test Results)," MwRSF Research Report No. TRP-03-179-07, Midwest Roadside Safety Facility, Lincoln, Nebraska (2007).

Hendrick03 Hendrick II, S.E., "*Determination of Mechanical Properties of Treated Wood using Near Infrared Spectroscopy*, Master's Thesis, University of Tennessee, Knoxville, TN (2003).

Hron11 Hron, J. and N. Yazdani, "Nondestructive Strength Assessment of In-Place Wood Utility Poles," *Journal of Performance of Constructed Facilities*, Vol. 25, No. 2 (April 2011).

104	Plaxico15	Plaxico, C.A. and M.H. Ray, "Effects of Guardrail Post Deterioration on the Crash
105		Performance of the G4(2W) Guardrail," *Transportation Research Record*, Paper
106		No. 15-xxx (in review), Transportation Research Board, Washington D.C. (2015).
107	Ray 15	Ray, M.H, C.A. Plaxico, C.E. Carrigan, and T.O. Johnson, "Criteria for Restoration
108		of Longitudinal Barriers, Phase II," Final Report, Project 22-28, National
109		Cooperative Highway Research Program, Washington, D.C. (expected 2015).
110	Tallavo09	Tallavo, F.J., *New Methodology for the assessment of Decayed Utility Wood Poles*
111		*Using Ultrasonic Testing*, Doctoral Thesis, University of Waterloo, Ontario,
112		Canada (2009).